The Journal of Chemical Physics

Experimental quantification of decoherence via the Loschmidt echo in a many spin system with scaled dipolar Hamiltonians

Cite as: J. Chem. Phys. **143**, 164308 (2015); https://doi.org/10.1063/1.4934221
Submitted: 01 July 2015 • Accepted: 08 October 2015 • Published Online: 26 October 2015

Lisandro Buljubasich, Claudia M. Sánchez, Axel D. Dente, et al.

Experimental quantification of decoherence via the Loschmidt echo in a many spin system with scaled dipolar Hamiltonians

Lisandro Buljubasich,[1,2] Claudia M. Sánchez,[2] Axel D. Dente,[1,2] Patricia R. Levstein,[1,2,a)] Ana K. Chattah,[1,2,b)] and Horacio M. Pastawski[1,2]
[1]*Instituto de Física Enrique Gaviola (IFEG-CONICET), Córdoba 5000, Argentina*
[2]*Facultad de Matemática, Astronomía y Física, Universidad Nacional de Córdoba, Ciudad Universitaria, Córdoba 5000, Argentina*

(Received 1 July 2015; accepted 8 October 2015; published online 26 October 2015)

We performed Loschmidt echo nuclear magnetic resonance experiments to study decoherence under a scaled dipolar Hamiltonian by means of a symmetrical time-reversal pulse sequence denominated Proportionally Refocused Loschmidt (PRL) echo. The many-spin system represented by the protons in polycrystalline adamantane evolves through two steps of evolution characterized by the secular part of the dipolar Hamiltonian, scaled down with a factor $|k|$ and opposite signs. The scaling factor can be varied continuously from 0 to 1/2, giving access to a range of complexity in the dynamics. The experimental results for the Loschmidt echoes showed a spreading of the decay rates that correlate directly to the scaling factors $|k|$, giving evidence that the decoherence is partially governed by the coherent dynamics. The average Hamiltonian theory was applied to give an insight into the spin dynamics during the pulse sequence. The calculations were performed for every single radio frequency block in contrast to the most widely used form. The first order of the average Hamiltonian numerically computed for an 8-spin system showed decay rates that progressively decrease as the secular dipolar Hamiltonian becomes weaker. Notably, the first order Hamiltonian term neglected by conventional calculations yielded an explanation for the ordering of the experimental decoherence rates. However, there is a strong overall decoherence observed in the experiments which is not reflected by the theoretical results. The fact that the non-inverted terms do not account for this effect is a challenging topic. A number of experiments to further explore the relation of the complete Hamiltonian with this dominant decoherence rate are proposed. [http://dx.doi.org/10.1063/1.4934221]

I. INTRODUCTION

Nuclear Magnetic Resonance (NMR) has an incomparable capacity to manipulate natural couplings that originate multiple spin dynamics, presenting a unique scenario for practical and theoretical studies. The observation of non-equilibrium many-body dynamics and the achievement of quantum time-reversal experiments along with the study of decoherence have attracted much attention in connection with fundamental problems, as the arrow of time and the quantum-classical limit.[1,2] Decoherence can be roughly defined as the degradation of the information contained in the quantum state used to describe a system. This could be the result of experimental imperfections, the interaction with an uncontrolled environment, or an oversimplified description of the system. In the last decades, these studies spanned from mesoscopic phenomena, thermalization, and the evaluation of decoherence to practical applications, such as testing quantum computation algorithms and developing strategies to extend the lifetime of quantum information.[3–12]

Time-reversal procedures and the generation of echoes in NMR[1] are ubiquitous since Hahn's pioneer work in the 1950s.[13] A Hahn echo is obtained when the lost transverse magnetization is recovered by the application of a short radio-frequency (r.f.) pulse. This pulse has the effect of reversing perturbations linear in spin operators, such the magnetic field inhomogeneities and the chemical shifts, that affect the precession of individual spins. Here, many-spin interactions constitute non-controlled terms that attenuate the echo amplitude. In the context of solid state NMR, the so-called *magic echo* (ME) was the first r.f. pulse sequence designed to reverse the homonuclear dipolar Hamiltonian, which is bilinear in the spin operators and provides a real many-body dynamics.[14] As in the Free Induction Decay (FID), the information stored in the global polarization rotating around the external magnetic field spreads out among multiple spin correlations named multiple quantum coherences (MQC).[15] Although the original ME was successful in recovering polarization, the results were recently improved by refining the experimental procedure.[16,17]

More subtle, the Polarization Echo (PE) defines a family of experiments where the locally injected initial condition diffuses under the dipolar Hamiltonian that conserves polarization.[18–20] In this process, the growth of correlations is produced among states with the same spin projection (zeroth-order coherences). In none of the ME, MQC, or PE experiments, the origin of the echo attenuation is fully clear. It has been suggested[21] that non-controlled interactions can act with

a)Deceased.
b)Author to whom correspondence should be addressed. Electronic mail: chattah@famaf.unc.edu.ar.

a decay estimated by the Fermi's Golden Rule,[22] or hidden beyond the complexity of the many-body dynamics in a perturbation independent regime.[23] In any case, Hahn echoes and magic echoes are nowadays essential components of numerous techniques in solid-state NMR, liquid state NMR, and NMR imaging among others applications. In particular, the *magic echo* pulse sequence is a standard tool to observe the dynamics in open quantum systems.[15,20,24,25]

All the mentioned experiments lead to the more general concept of the Loschmidt echo (LE).[26–29] A LE can be defined as the retrieval of an excitation after decaying due to a quantum evolution, through a time-reversal procedure that involves the sign change of the Hamiltonian. Then, LE arises as a good quantifier of decoherence, since the signal revival is limited by uncontrolled and non-inverted Hamiltonian terms, environmental interactions, or experimental imperfections. A notable result for the LE occurs when the dynamics is complex, i.e., in a system with a chaotic classical version. The time scale of the decay can be identified with a Lyapunov exponent associated to the controlled part of the dynamics, leading to an intrinsic decoherence or perturbation-independent regime.[2,26]

The concept of LE has been implemented in a wealth of experimental and theoretical techniques.[11,28,30] For many-body spin systems, it results an essential tool harnessing the elusive localization phenomenon.[29,31–33] In the NMR context, LE procedures have been studied for a variety of systems and evolutions.[19,32,34–37] Generally, it has been observed that the decoherence rate increased with the number of dynamically coupled spins.[38–40] This trend is consistent with the hypothesis that guides our work in the field, i.e., the fact that natural instabilities associated with the intrinsic chaos of a many spin system could make the uncontrolled parameters to be able to produce an intrinsic decoherence rate, which scales proportionally with the Hamiltonian that generates the spin dynamics.[20,24,41]

At this point, two experiments are worth mentioning related to the possibility of achieving a fine tuning of the dynamics through *on-resonance* and *off-resonance* irradiation. In a cross-polarization experiment, thermalization of the rare (^{13}C) spins is produced by the abundant (^{1}H) proton system. On-resonance irradiation during acquisition produces optimal results, i.e., more dynamics in the proton system produces faster thermalization.[19,42,43] Conversely, a carbon-proton system can be isolated by irradiating protons in the Lee-Goldburg (LG) (off-resonance) condition to cancel out the homonuclear dynamics. In that case, although the polarization does not spread into the proton system, i.e., the system does not fully thermalize, the decoherence remains in the same time scale. These experiments opened the question whether decoherence is dominated by the original dipolar Hamiltonian.[20]

A somewhat inconvenient feature of the ME and PE experiments implemented to study decoherence is the lack of symmetry in the pulse sequences and their underlying physical implications: the *backward* evolution lasts twice as long as the *forward* evolution. This asymmetry also correlates with the different relative importance of the truncated terms, which are the candidates to account for decoherence. Thus, we seek for an implementation of time reversal that could equally scale down the secular components of the Hamiltonian as well as the non-secular ones, making physically equivalent the *forward* and *backward* evolutions. In this paper, continuous r.f. irradiation periods with different *off-resonance* frequencies are used to produce dipolar Hamiltonians scaled down by factors that can be varied from $-1/2$ to 1. We implement this procedure in polycrystalline adamantane. Our experiments belong to the ME family, since the effective r.f. field is always at 90° with respect to the polarization.

The rest of the paper is organized as follows: in Section II, a short revision of the effect of continuous *off-resonance* r.f. irradiation on the coupled many-spin system is presented (Sec. II A), followed by the introduction of the new pulse sequence and a theoretical survey of the mechanisms to achieve time reversion (Sec. II B). Section III A includes a brief description of the sample used in the experiments, a number of tests performed to quantify the effects of r.f. inhomogeneities, and a list of the most relevant experimental details. Section III B is the central part of the paper. Here, the experimental results acquired with different scaling factors are presented and discussed. While decoherence rates spread correlating directly to the scaling factors, there is a strong overall decoherence not accounted by the non-inverted terms. In Section III C, we explore the effect of many spin dynamics by analysing the pulse sequence with the help of the average Hamiltonian theory. Finally, in Sec. IV, the conclusions of our work are listed along with suggested experiments that might help in understanding the relatively weak dependence of decoherence from the scaled Hamiltonian as well as the role of the whole Hamiltonian.

II. TIME REVERSAL PULSE SEQUENCE

A. Scaling the dipolar Hamiltonian

Let us consider a system of N mutually interacting spins-1/2 in the presence of a strong external magnetic field $\mathbf{B}_0 = B_0\hat{z}$, under off-resonance r.f. irradiation with angular frequency ω. The Hamiltonian (in frequency units) referred to a frame rotating with $\omega_0 = \gamma B_0$ can be expressed as

$$\mathcal{H} = -\Omega I^z - \omega_1 I^x + \mathcal{H}_{\rm d}^z + \mathcal{H}_{\text{d-NS}}^z, \tag{1}$$

where $\omega_1 = \gamma B_1$ is the intensity of the r.f. field in rad/s, $\Omega = \gamma b_0 = \omega_0 - \omega$ is the off-resonance (see Fig. 1(a)), and $I^\alpha = \sum_i I_i^\alpha$ (with $\alpha = x, y, z$) are the total spin operators. The dipolar Hamiltonian $\mathcal{H}_{\rm d}^z$ is

$$\mathcal{H}_{\rm d}^z = \sum_{i<j} d_{ij}(3I_i^z I_j^z - \mathbf{I}_i \cdot \mathbf{I}_j), \tag{2}$$

where $d_{ij} = \frac{\mu_0}{4\pi}\frac{\gamma^2\hbar}{r_{ij}^3}\frac{(1-3\cos^2\vartheta_{ij})}{2}$, $\mathbf{r}_{ij}$ is the internuclear vector, and ϑ_{ij} the angle between $\mathbf{r}_{ij}$ and the external magnetic field direction. The term $\mathcal{H}_{\text{d-NS}}^z$ corresponds to non-secular interactions (terms C to F in the alphabet notation[44]) which although containing pre-factors of the same order as $\mathcal{H}_{\rm d}^z$ result truncated by B_0 and hence are disregarded as usual. Indeed, the 0-th order wave function in the laboratory frame has a correction from second order perturbation theory that results proportional to the ratio between the dipolar local fields and the external magnetic field, typically $\sim 10^{-4}$.[44] If the effective frequency,

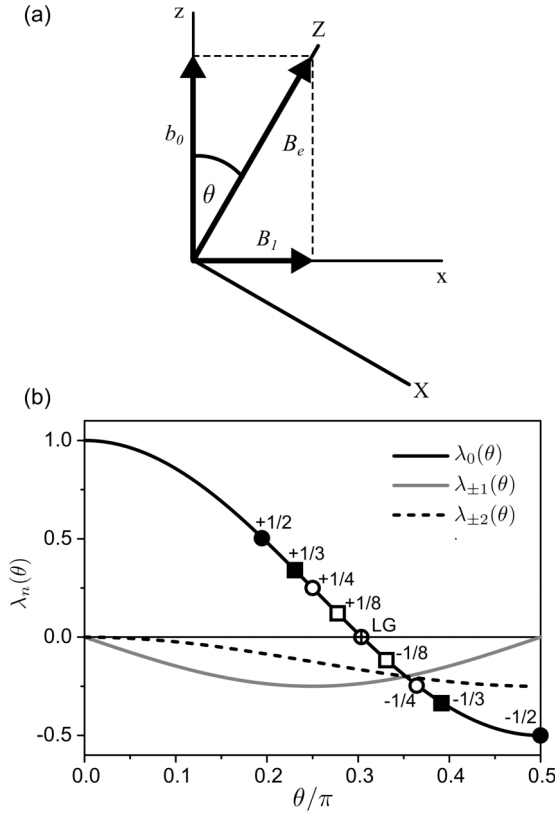

FIG. 1. (a) The rotating and *tilted* frames with the relevant fields involved. (b) Behaviour of the pre-factor λ's as a function of θ, i.e., the angle between z-axis and the Z-axis of the rotating and tilted frames, respectively.

$\omega_e = \sqrt{\omega_1^2 + \Omega^2}$, is much larger than the local dipolar couplings, i.e., $\omega_e \gg d_{ij}\,\forall i,j$, it is convenient to define a new quantization axis Z along the effective field, which forms an angle θ with the direction of the external magnetic field, $\hat{z}$. Then, the Hamiltonian of Eq. (1) can be rewritten, referred to this *tilted frame*, as[44]

$$\mathcal{H} = -\omega_e I^Z + \sum_{M=-2}^{+2} \lambda_M(\theta)\mathcal{H}_M^Z. \tag{3}$$

The factors on the second term in the right-hand side of Eq. (3) are listed in Table I. Retaining only the secular part with respect to the tilted frame (X,Y,Z), we have

$$\mathcal{H} = -\omega_e I^Z + \frac{1}{2}(3\cos^2\theta - 1)\sum_{i<j} d_{ij}(3I_i^Z I_j^Z - \mathbf{I}_i\cdot\mathbf{I}_j). \tag{4}$$

Figure 1(b) shows the behaviour of λ factors as a function of θ within the range $[0,\pi/2]$. The sign change of λ_0 opens the

TABLE I. Functional form of $\mathcal{H}_M^Z$ and λ_M.

M	H_M^Z	$\lambda_M(\theta)$
0	$\sum_{i<j} d_{ij}(3I_i^Z I_j^Z - \mathbf{I}_i\cdot\mathbf{I}_j)$	$\frac{1}{2}(3\cos^2\theta - 1)$
+1	$\sum_{i<j} 3d_{ij}(I_i^+ I_j^Z + I_i^Z I_j^+)$	$-\frac{1}{2}\sin\theta\cos\theta$
−1	$\sum_{i<j} 3d_{ij}(I_i^- I_j^Z + I_i^Z I_j^-)$	$-\frac{1}{2}\sin\theta\cos\theta$
+2	$\sum_{i<j} 3d_{ij}(I_i^+ I_j^+)$	$\frac{1}{4}\sin^2\theta$
−2	$\sum_{i<j} 3d_{ij}(I_i^- I_j^-)$	$\frac{1}{4}\sin^2\theta$

possibility of achieving the time reversion. This fact was first pointed out by Pines and co-workers back in 1972. The authors introduced a pulse sequence, known as *the magic echo*,[14,45,46] consisting on a block of free evolution under $\mathcal{H}_d^z$, followed by a block of on-resonance irradiation lasting twice as much as the first block, which produces an effective evolution under $-\mathcal{H}_d^z/2$.

We present here a new pulse sequence with time symmetry to generate an echo with two blocks of off-resonance r.f. irradiation. Each block produces a scaling of the dipolar couplings d_{ij} by factors λ_0 with the same magnitude and opposite signs (see Fig. 1(b)) leading to the time reversion of the evolution. By controlling the r.f. power and frequency (i.e., the angle θ), $|\lambda_0|$ can be continuously varied from 1/2 to 0. The lower value, $\lambda_0 = 0$, corresponds to the well-known LG condition, achieved with off-resonance irradiation such that $\theta = 54.7°$, the magic angle.

B. Time symmetrical pulse sequence

The proposed pulse sequence is shown in Fig. 2. To describe the effect on the spin dynamics, we focus on the propagators $\mathcal{U}_F$ and $\mathcal{U}_B$ corresponding to the *forward* and *backward* blocks.

Let us consider first the *forward* block, consisting in off-resonance irradiation during τ with an effective axis $\pm Z_F$ surrounded by hard pulses $(\beta_F)_{\overline{y}}$ and $(\beta_F)_y$, such that $|\beta_F| = 90° - \theta$. Considering the Hamiltonian of Eq. (4), i.e., the Hamiltonian including only *secular* terms during the off-resonance irradiation period, the propagator can be written as

$$\begin{aligned}\mathcal{U}_F^{\text{sec.}}(\tau) = \exp(-i\beta_F I^y) \\ \times \exp\left[-i\left(-\omega_e I^{Z_F} + \lambda_0(\theta_F)\mathcal{H}_0^{Z_F}\right)\frac{\tau}{2}\right] \\ \times \exp\left[-i\left(\omega_e I^{Z_F} + \lambda_0(\theta_F)\mathcal{H}_0^{Z_F}\right)\frac{\tau}{2}\right] \\ \times \exp(i\beta_F I^y).\end{aligned} \tag{5}$$

As $[I^{Z_F}, \mathcal{H}_0^{Z_F}] = 0$, the sign change of the phase and the off-resonance frequency at the middle of the r.f. irradiation block (see Fig. 2) eliminates the precession with ω_e, leaving the propagator as

$$\begin{aligned}\mathcal{U}_F^{\text{sec.}}(\tau) = \exp(-i\beta_F I^y)\exp\left(-i\lambda_0(\theta_F)\mathcal{H}_0^{Z_F}\tau\right) \\ \times \exp(i\beta_F I^y).\end{aligned} \tag{6}$$

The pulses $\pm\beta_F$ produce a global rotation of the Hamiltonian onto the x-axis of the rotating frame, yielding

$$\mathcal{U}_F^{\text{sec.}}(\tau) = \exp\left(-i\lambda_0(\theta_F)\mathcal{H}_0^x\tau\right), \tag{7}$$

where $\mathcal{H}_0^x$ represents the Hamiltonian $\mathcal{H}_0^{Z_F}$ after such transformation.

The backward block consists of off-resonance irradiation during τ with effective axes $\pm Z_B$ surrounded by pulses $\pm\beta_B$. Repeating the reasoning of the previous lines, we find that the backward block is characterized by the propagator,

$$\mathcal{U}_B^{\text{sec.}}(\tau) = \exp\left(-i\lambda_0(\theta_B)\mathcal{H}_0^x\tau\right). \tag{8}$$

The total evolution propagator at the end of the second block is

$$\begin{aligned}\mathcal{U}^{\text{sec.}}(2\tau) &= \mathcal{U}_B^{\text{sec.}}(\tau)\mathcal{U}_F^{\text{sec.}}(\tau) \\ &= \exp\left\{-i\left[\lambda_0(\theta_F) + \lambda_0(\theta_B)\right]\mathcal{H}_0^x\tau\right\}.\end{aligned} \tag{9}$$

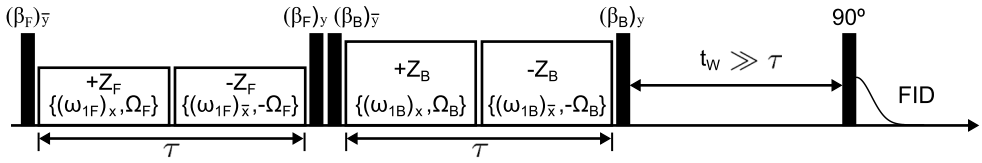

FIG. 2. Time reversal pulse sequence, consisting in two blocks of *forward* and *backward* evolutions. Each block is composed by two periods of continuous r.f. irradiation surrounded by hard pulses. The waiting period t_W is included to allow any spurious transverse magnetization to dephase before the acquisition of the FID.

If the r.f. intensity and the off-resonance frequency in each block are adjusted to fulfil $\lambda_0(\theta_F) = -\lambda_0(\theta_B)$, the initial condition is recovered at 2τ, obtaining an echo. In other words, $\mathcal{U}^{\text{sec.}}(2\tau) = \mathcal{U}_B^{\text{sec.}}(\tau)\mathcal{U}_F^{\text{sec.}}(\tau) = \mathcal{I}$.

The initial condition is the high temperature thermal equilibrium density operator, $\rho(0) \propto I^z$. The waiting period labelled as t_W in Fig. 2 is included to let spurious coherences generated during the sequence to dephase prior to the signal acquisition. Denoting the total propagator by $\mathcal{U}(2\tau) = \mathcal{U}_B(\tau)\,\mathcal{U}_F(\tau)$, the signal obtained after the last 90° pulse results in

$$\begin{aligned} S_{LE}(2\tau) &= \text{Tr}\left(I^x \mathcal{U}_{\pi/2}\mathcal{U}(2\tau) I^z \mathcal{U}^{-1}(2\tau)(\mathcal{U}_{\pi/2})^{-1}\right) \\ &= \text{Tr}\left(I^z\, \mathcal{U}(2\tau) I^z \mathcal{U}^{-1}(2\tau)\right). \end{aligned} \tag{10}$$

If the dynamics is restricted to only secular terms, i.e., $\mathcal{U} \equiv \mathcal{U}^{\text{sec.}}$, Eq. (10) yields $S_{LE}(2\tau) = 1$. However, perturbations to the secular evolution during off-resonance irradiation are introduced by the non-secular terms of the Hamiltonian of Eq. (3), along with experimental imperfections and inhomogeneity in the magnetic fields (either static or r.f. fields). As a result, the perfect reversion is never achieved. Defining the *scaling factor* $k = \lambda_0$, the complete evolution is more realistically characterized by a total propagator,

$$\begin{aligned} \mathcal{U}(2\tau) = &\exp\left[-i\tau\left(-|k|\mathcal{H}_0^x + \Sigma_B\right)\right] \\ &\times \exp\left[-i\tau\left(|k|\mathcal{H}_0^x + \Sigma_F\right)\right]. \end{aligned} \tag{11}$$

Although the Σ's have an explicit relationship with k (see Fig. 1), they do not change the sign within the whole range of variation of k. Thus, they are collected as uncontrollable terms in the above equation.

We will refer to the pulse sequence shown in Fig. 2 as PRL echo, where the acronym stands for Proportionally Refocused Loschmidt echo.

III. RESULTS AND DISCUSSION

A. Experimental details

1. The sample

The experiments were performed on polycrystalline adamantane, a plastic crystal in which the ^{1}H spins form a dipole-coupled many-spin system. The rapid and isotropic tumbling of the molecules in adamantane at room temperature average out intramolecular dipole-dipole interactions as well as chemical shift anisotropy.[48] The isotropic chemical shift is $\lesssim$100 Hz, too small to be detected in solid state NMR.[35] Therefore, adamantane can be considered as a spherical molecule with its 16 protons placed, on average, at the center of the molecule, with only intermolecular dipole-dipole interactions. The molecules are located in a face-centred cubic lattice, so that each ^{1}H is coupled to 16 ^{1}H's placed at the positions of the 12 nearest molecules, resulting in 192 nearest-neighbours (separated 0.67 nm).[49] Further neighbours are at 0.93 nm, 1.14 nm, etc.[50] The static ^{1}H NMR spectrum of adamantane is close to a Gaussian shape with a linewidth of ~12 kHz, which corresponds to a effective dipolar coupling strength of $d_e \sim 5.7$ kHz.[49]

2. Testing the scaling Hamiltonian blocks

All the experiments were carried out in a Bruker Avance II spectrometer operating at 300 MHz Larmor frequency. Given a scaling factor $|k|$ in the pulse sequence of Fig. 2, two angles are determined for $+k$ and $-k$, except for $k = 0$. To obtain the same effective field ($B_e = \gamma\omega_e$) in the forward and backward blocks, the r.f. intensity and the off-resonance need to be carefully adjusted. Therefore, the knowledge of the r.f. coil performance and an estimation of the effect of r.f. inhomogeneities in the results becomes highly relevant. A series of test were carried out to explore the performance of different parts of the PRL echo sequence. Figure 3(a) shows the pulse sequence used for an off-resonance nutation. A block of continuous r.f. of intensity ω_1 out-of-resonance by a quantity Ω is surrounded by two β pulses to produce a net rotation around the x-axis of the rotating frame, with a frequency ω_e. The signal intensity as a function of τ is a damped oscillatory function. During the FID, the magnetization evolving with magnetic field inhomogeneities and dipolar couplings decays exhibiting a Gaussian shape for this sample.[49] Thus, it is natural to assume that the decay during the nutation, which is a measure of the r.f. inhomogeneity and the dipolar interaction, follows the same shape. The experimental data were fitted with the following expression:

$$S(\tau) = A + B\sin(\omega_e\tau + \phi_0)\, e^{-(\tau/\tau_0)^2}, \tag{12}$$

which reproduced the experimental results with high accuracy.

By varying Ω for constant ω_1 (i.e., θ is modified), it is possible to perform nutations with different dipolar scaling factors k. The plot in Fig. 3(a) presents four group of experiments, where the r.f. power was varied to cover the range which will be used in the experiment of Sec. III A 3. Additionally, Ω was set to obtain $k = 0, \pm1/2, \pm1/3, \pm1/4, \pm1/5, \pm1/6, \pm1/7, \pm1/8$. The effective decay times obtained from the fittings, τ_0's, are plotted against the scaling factor. The effect of r.f. inhomogene-

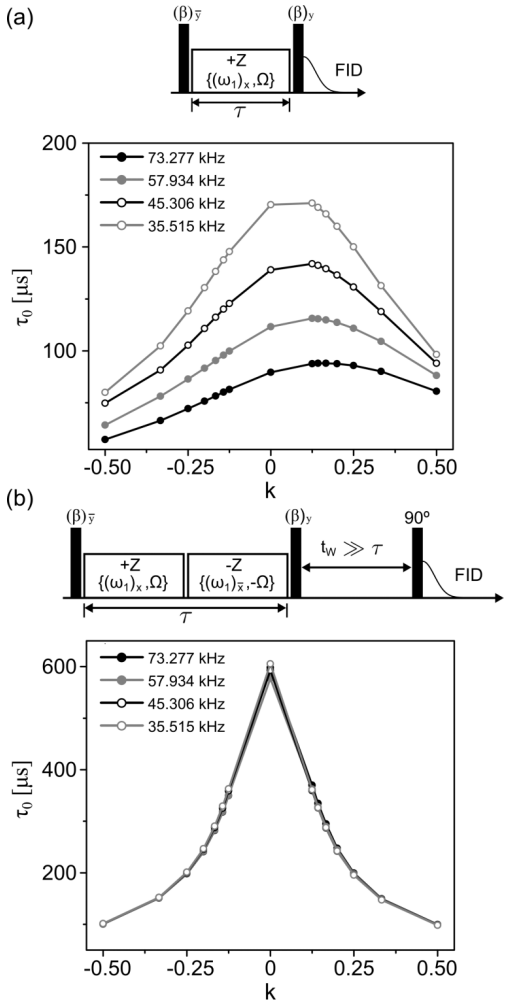

FIG. 3. Tests to quantify the effects of r.f. inhomogeneities in the signal decay. Pulse sequences and experimental results for (a) the off-resonance nutations with different r.f. powers and (b) the off-resonance nutations with phase inversion of the r.f. in the middle of the evolution.

ities becomes evident by the fact that for weaker power, larger values of τ_0's are obtained at fixed k. On the other hand, at fixed r.f. power, smaller k values will result in larger τ_0's too, because the dipolar evolution is proportionally smaller. However, there should be no difference if the evolution is driven with $+k$ or $-k$. The lack of symmetry of these curves is another symptom of the presence of r.f. inhomogeneities.

The blocks of r.f. with opposite phases in each part of PRL echo serve two purposes: in the first place, the particular arrangement is included to refocus evolutions with the Zeeman Hamiltonian in the tilted frame (i.e., $\propto \omega_e I^Z$). As a side effect, it also attenuates the effects of the r.f. inhomogeneity. To quantify the performance of the phase inversion with our probe and sample, and more important, in the range of intensities we are dealing with, experiment with the sequence shown in Fig. 3(b) was carried out. The experimental results (Fig. 3(b)) display the behaviour of the corresponding decay times. Notice that, due to the reversion of the Zeeman evolution, after the $(\beta)_y$-pulse, the magnetization should lay along the z-axis of the rotating frame. Then, a waiting time and a read-out 90° pulse were added, similarly to the case of PRL echo.

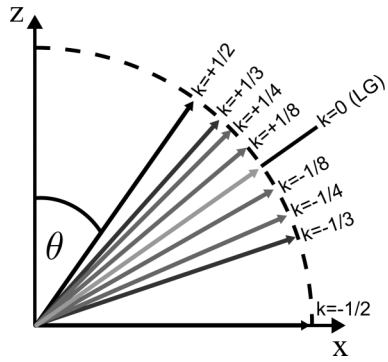

FIG. 4. The angles of the effective field for different k schematically represented. The dashed line shows that all vectors have the same length.

The decay times τ_0 with this pulse sequence show curves which are symmetric in k as expected, with minor differences as the r.f. power varies, confirming that any r.f. inhomogeneities are essentially removed. Consistently, the τ_0 values are more than three times larger than in the previous case. At constant k, the dispersion of τ_0's by varying the power is ~2% for $k = 0$ and $\lesssim 1\% \; \forall k \neq 0$. The discrepancy between values corresponding to $\pm k$ is always <2% independently of the r.f. intensity.

This analysis shows that the PRL echo sequence of Fig. 2 can be reliably implemented to generate time-reversal Hamiltonians with scaled dipolar dynamics, as the blocks with different r.f. power do not introduce any extra decay rate via r.f. inhomogeneities. It is worthy to remark, once again, that this conclusion is true for the probe, the sample geometry, and the range of power used in our experiments.

3. *Experiments with PRL echo for different k*

Figure 4 shows the inclination of the tilted frame with respect to the rotating frame for the k values covered in the experiments of Sec. III B. The effective field strength, B_e, was maintained constant independently of k, as indicated by the dotted line. The range of values of the relevant quantities used in the experiments are summarized in Table II. The resulting effective field was $B_e/2\pi = 73.277$ kHz with a maximum discrepancy with respect to the theoretical value $\lesssim 1\%$. In all cases, the waiting time before the reading pulse, in order to allow unwanted transverse magnetization to decay, was set to $t_w = 3$ ms, whereas $\tau \leq 1$ ms was varied in steps of 13.6 μs, i.e., such that $\omega_e \tau = 2n\pi$, to be consistent with the average Hamiltonian theory.[45,51] All the *hard r.f. pulses* were shorter than 4.5 μs, much shorter than the minimum step of the forward and backward blocks. The experiments were acquired with 144 scans to improve the signal-to-noise ratio.

TABLE II. Range of variation of the parameters during the experiments.

Parameter	Minimum	Maximum
$\omega_1/2\pi$ (kHz)	(42.306 ± 0.005)	(73.277 ± 0.005)
$\Omega/2\pi$ (kHz)	0	(60.137 ± 0.001)
β (μs)	(0.97 ± 0.01)	(2.65 ± 0.01)

B. Loschmidt echoes with different dipolar scaling factors

The PRL echo pulse sequence (Fig. 2) produces a scaling of the secular part of the dipolar Hamiltonian with respect to the tilted frame, i.e., $\lambda_0 \mathcal{H}_0^Z$. Therefore, for every scaling factor $|k|$, it is expected a similar dynamics with a modified time scale. By varying the offset frequency and the r.f. power, a set of echoes as a function of τ were acquired with different $|k|$ values. The experimental results are summarized in Fig. 5. In all cases, there is a forward evolution with a factor $k = +1/n$ followed by a backward evolution with $k = -1/n$ for $n = 2, 3, 4, 8$. In the particular case of the Lee-Goldburg condition,[44] where $k = 0$, there is no need for a backward block to obtain zero secular Hamiltonian evolution. Two blocks with exactly the same parameters were used, however, to keep the same timing in the pulse sequence for all the experiments, for the sake of comparison.

In Fig. 5(a), $S_{LE}(2\tau)$ is plotted against τ, the duration of the forward evolution. The curves show the same decay for $0 < \tau \lesssim 400\ \mu$s, whereas for further evolution times, the echoes behave appreciably different. The smaller the $|k|$ value, the weaker the rate of decay, and all curves lay below the limiting case $|k| = 0$. Thus, the curve corresponding to LG can be taken as a reference for the decays with $|k| \neq 0$. In Fig. 5(b) the data are presented renormalized to the LG curve. The dissimilarity between the echoes, directly related to the strength of the secular evolutions, becomes clearer in this plot. This trend is remarkable as the decay that is in principle associated with the non-secular terms of the scaled dipolar evolution (i.e., $\mathcal{H}_M^x$ with $M = \pm 1, \pm 2$) and uncontrolled experimental instabilities.

In other words, the decoherent behaviour of the system observed in the decay of the S_{LE} for $\tau \gtrsim 400\ \mu$s is intrinsically related to the coherent dynamics dictated by the scaled secular Hamiltonian. This can be, however, understood as follows: given a time value, τ, forward evolutions driven by stronger secular Hamiltonians take the spin system to a more complex final state, making the reversion more imperfect. The behaviour of the S_{LE} is a manifestation of such effect, and can be observed because the experimental errors (e.g., r.f. inhomogeneities) are reduced to the minimum.

As the smaller the scaling factor the slower the spin dynamics under the secular Hamiltonian, it is convenient to define a quantity $\phi = k\tau$ to account for this difference. Figure 5(c) displays the behaviour of the echoes against ϕ. Notice that the curve corresponding to the Lee-Goldburg condition is excluded, because the definition of the time scale yields $\phi \equiv 0$. The curves with smaller $|k|$ decay faster in this case.

Figure 5(d) displays the results shown in (b) against ϕ, to emphasize that, for a short forward evolution durations, the curves are superimposed meaning that the states of the system for different k are similar. For longer evolutions (e.g., ϕ

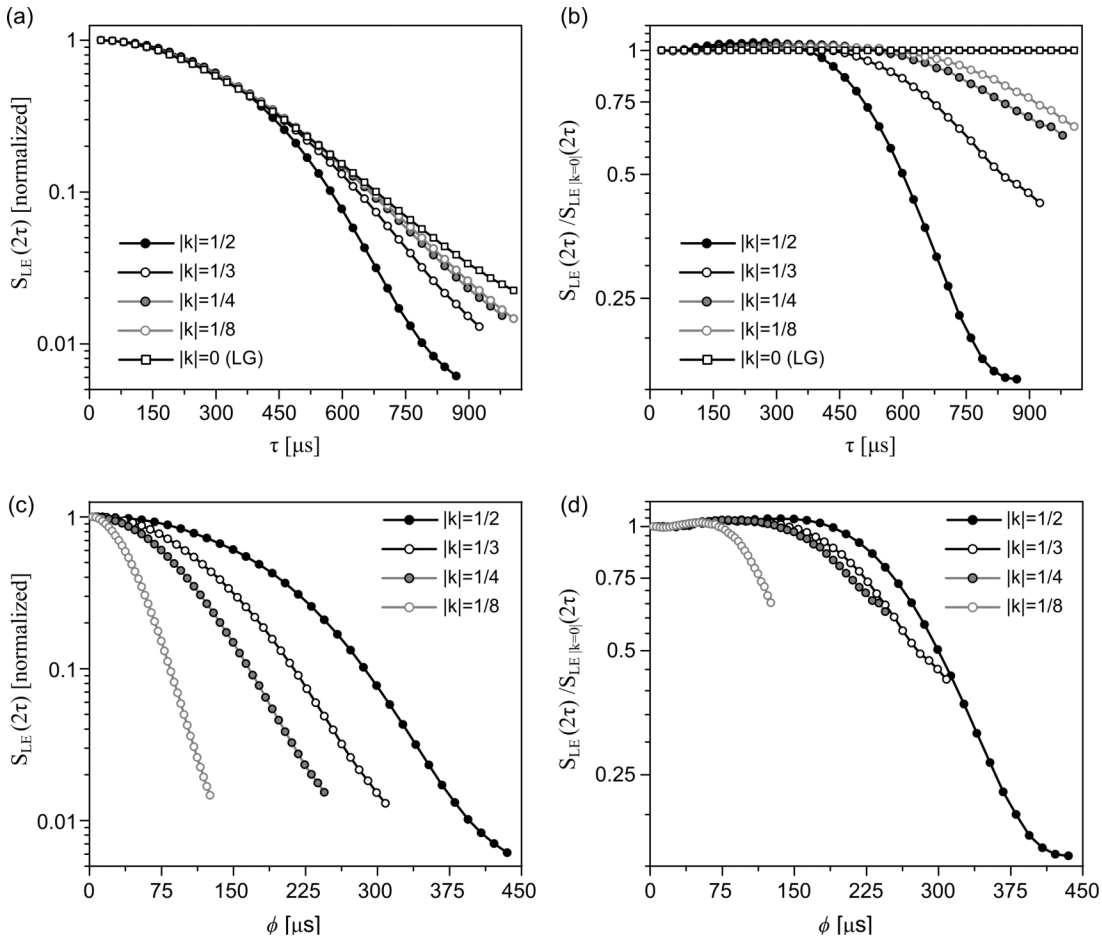

FIG. 5. (a) Loschmidt echoes with different scaling factors, $|k|$. (b) The curves shown in (a) normalized with the curve corresponding to $k = 0$. (c) Echoes plotted against $\phi = k\tau$ (the curve with $k = 0$ is excluded). (d) Curves displayed in (b) plotted against the new time scale ϕ.

> 70 μs), the discrepancies due to non-secular dynamics become more relevant, accentuating the imperfections in the inversion.

C. Analysis based on the average Hamiltonian theory

1. Theory

We will explore here the effect of the non-secular terms in Eq. (3) during the r.f. irradiation. The problem lends itself to be treated in the context of the average Hamiltonian theory.[53]

Let us consider a single blocks of arbitrary off-resonance r.f. with the effective field aligned with the Z-axis of the tilted frame, as shown in Fig. 6(a). The spins evolve under the Hamiltonian of Eq. (3), which has the general form,

$$\mathcal{H} = \mathcal{H}_{\rm e}(t) + \mathcal{H}_{\rm d}^{Z}, \tag{13}$$

where the explicit time dependency is on the r.f. Hamiltonian. The propagator associated with $\mathcal{H}_{\rm e}(t)$ is expressed as

$$\mathcal{U}_{\rm e}(t) = \mathbf{T}\,\exp\left\{-i\int_0^t \mathcal{H}_{\rm e}(t')dt'\right\}, \tag{14}$$

$\mathbf{T}$ being the Dyson time-ordering operator. The density operator $\rho(t)$ evolves with the total propagator,

$$\mathcal{U}(t) = \mathcal{U}_{\rm e}(t)\mathcal{U}_{\rm d}^{Z}(t), \tag{15}$$

where

$$\mathcal{U}_{\rm d}^{Z}(t) = \mathbf{T}\,\exp\left\{-i\int_0^t \widetilde{\mathcal{H}}_{\rm d}^{Z}(t')dt'\right\}. \tag{16}$$

The Hamiltonian $\widetilde{\mathcal{H}}_{\rm d}^{Z}(t)$ is the *toggling frame Hamiltonian*, $\widetilde{\mathcal{H}}_{\rm d}^{Z}(t) = \mathcal{U}_{\rm e}^{-1}(t)\mathcal{H}_{\rm d}^{Z}\mathcal{U}_{\rm e}(t)$. As the r.f. Hamiltonian is cyclic, with cycle time $\tau_c = 2\pi/\omega_e$ (see Fig. 6(a)), the total propagator fulfils[44,52,53]

$$\mathcal{U}(n\tau_c) = \mathcal{U}_{\rm d}^{Z}(n\tau_c). \tag{17}$$

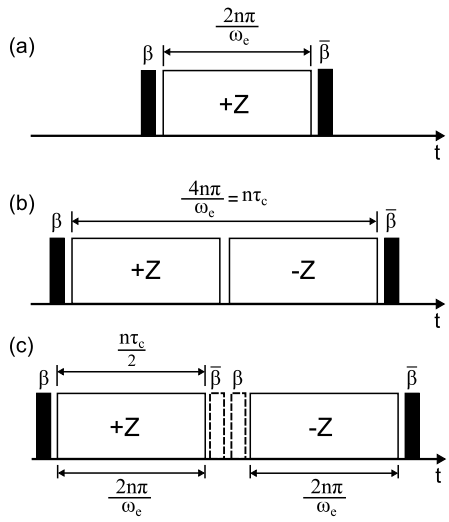

FIG. 6. (a) Scheme used to compute the first two orders of the average Hamiltonian. (b) The way in which the calculations are customarily performed in several publications. A single time propagator is calculated considering the pair of r.f. blocks with opposite phases. (c) The alternative way proposed here: the total propagator is rendered from propagators calculated on each single r.f. block.

Then, in n cycles, the result can be written in a form of a single exponential by means of the Magnus expansion,

$$\mathcal{U}_{\rm d}^{Z} = \exp\left\{-i\,n\tau_c\sum_{i=0}^{\infty}\overline{\mathcal{H}}^{(i)}\right\}, \tag{18}$$

where the first terms of the series are[44,52,53]

$$\overline{\mathcal{H}}^{(0)} = \frac{1}{\tau_c}\int_0^{\tau_c} dt'\widetilde{\mathcal{H}}_{\rm d}^{Z}(t'),$$
$$\overline{\mathcal{H}}^{(1)} = \frac{-i}{2\tau_c}\int_0^{\tau_c} dt''\int_0^{t''} dt'\left[\widetilde{\mathcal{H}}_{\rm d}^{Z}(t''),\widetilde{\mathcal{H}}_{\rm d}^{Z}(t')\right].$$

2. Computing the first orders

We have computed the first two orders with the Hamiltonians shown in Eq. (3) (and Table I), for a general inclination θ of the tilted frame with respect to the rotating frame (i.e., for a generic pair of values ω_1 and Ω). The first term in the expansion results

$$\overline{\mathcal{H}}^{(0)} = \lambda_0\mathcal{H}_0^{Z}, \tag{19}$$

i.e., the part of the dipolar Hamiltonian commuting with the Zeeman Hamiltonian $\propto I^{Z}$, as expected (in other words, the secular part). The next order, $\overline{\mathcal{H}}^{(1)}$, can be split into two expressions. In Eq. (20), all the terms including $\mathcal{H}_0^{Z}$ are collected,

$$\overline{\mathcal{H}}_{0,M}^{(1)} = -\frac{\lambda_0\lambda_1}{\omega_e}\left(\left[\mathcal{H}_0^{Z},\mathcal{H}_{+1}^{Z}\right]-\left[\mathcal{H}_0^{Z},\mathcal{H}_{-1}^{Z}\right]\right)$$
$$-\frac{\lambda_0\lambda_2}{2\,\omega_e}\left(\left[\mathcal{H}_0^{Z},\mathcal{H}_{+2}^{Z}\right]-\left[\mathcal{H}_0^{Z},\mathcal{H}_{-2}^{Z}\right]\right), \tag{20}$$

whereas $\overline{\mathcal{H}}_{M^2}^{(1)}$ involves commutation between the remaining non-secular terms, as seen in the following:

$$\overline{\mathcal{H}}_{M^2}^{(1)} = -\frac{(\lambda_1)^2}{\omega_e}\left[\mathcal{H}_{+1}^{Z},\mathcal{H}_{-1}^{Z}\right]-\frac{(\lambda_2)^2}{2\,\omega_e}\left[\mathcal{H}_{+2}^{Z},\mathcal{H}_{-2}^{Z}\right]. \tag{21}$$

Full expressions in terms of product operators are presented in Table III of the Appendix, where the commutators have been calculated for a system of N-interacting spins. The separation into two first order Hamiltonians is not arbitrary. In fact, $\overline{\mathcal{H}}_{0,M}^{(1)}$ is constructed with single- and double-quantum operators, which mix states from subspaces with different total angular momentum number, separated by an energy of the order of ω_e. In contrast, $\overline{\mathcal{H}}_{M^2}^{(1)}$ presents only zero- quantum operators, which mix states with nearly the same energy. Therefore, the effect of $\overline{\mathcal{H}}_{0,M}^{(1)}$ will be negligible as the frequency values are as large as experimentally possible on behalf of secularization. In what follows, we will drop this term and keep only $\overline{\mathcal{H}}_{M^2}^{(1)}$ as the first order of the average Hamiltonian. The pulses $\pm\beta$ surrounding the r.f. blocks in Fig. 6(a) switch the Hamiltonians from the tilted to the rotating frame. The zeroth- and first-order of the average Hamiltonian results, therefore, in

$$\tilde{\mathcal{H}}^{(0)} = \lambda_0\mathcal{H}_0^{x},$$
$$\tilde{\mathcal{H}}^{(1)} = -\frac{(\lambda_1)^2}{\omega_e}\left[\mathcal{H}_{+1}^{x},\mathcal{H}_{-1}^{x}\right]-\frac{(\lambda_2)^2}{2\,\omega_e}\left[\mathcal{H}_{+2}^{x},\mathcal{H}_{-2}^{x}\right], \tag{22}$$

where $\tilde{\mathcal{H}}^{(n)}$ are referred to the rotating frame, in contrast to $\overline{\mathcal{H}}^{(n)}$ which are referred to the tilted frame of reference. This

result is related to the decay rates obtained with the Fermi's Golden Rule approach.[47] In that context, the resulting decay rates are second order in the perturbation terms $\Sigma_{F,B}$ (see Eq. (11)), i.e., $\propto \lambda_j^2/\omega_e$.

3. Dynamics during the PRL echo sequence

To the best of our knowledge, since the publication of Rhim, Pines, and Waugh,[45] it is customary to compute the average Hamiltonians considering both r.f. blocks with opposite phases as the cycle, as shown in Fig. 6(b). Proceeding in that manner, the first-order is nullified by the change of the r.f. phase at the middle of the cycle,

$$\tilde{\mathcal{H}}^{(1)} = 0. \tag{23}$$

In contrast, we compute here the propagator for the PRL echo pulse sequence in terms of average Hamiltonians (see Fig. 2) in an alternative way. The strategy is depicted in Fig. 6(c): we calculate the average Hamiltonian terms for any block of r.f. with a specific phase by means of Eqs. (22). Two extra β pulses are introduced in the calculations to ensure that the result for all the blocks are referred to the x-axis of the rotating frame and fulfil the condition of Eq. (17) (in dashed lines in Fig. 6(c) to emphasize that they are included only for a mathematical purpose). The PRL echo propagator at times $\tau = 2n\tau_c$ is rendered from the blocks propagators as

$$\begin{aligned}\mathcal{U}(2n\tau_c) = \mathcal{U}_B^{(-)}(n\tau_c/2) \times \mathcal{U}_B^{(+)}(n\tau_c/2) \\ \times \mathcal{U}_F^{(-)}(n\tau_c/2) \times \mathcal{U}_F^{(+)}(n\tau_c/2),\end{aligned} \tag{24}$$

where (±) denotes the r.f. phase. Introducing the explicit form of the blocks propagators, one obtains

$$\begin{aligned}\mathcal{U}(2n\tau_c) = &\exp\left\{-i(\tilde{\mathcal{H}}_B^{(0)} - \tilde{\mathcal{H}}_B^{(1)})\frac{n\tau_c}{2}\right\} \\ &\times \exp\left\{-i(\tilde{\mathcal{H}}_B^{(0)} + \tilde{\mathcal{H}}_B^{(1)})\frac{n\tau_c}{2}\right\} \\ &\times \exp\left\{-i(\tilde{\mathcal{H}}_F^{(0)} - \tilde{\mathcal{H}}_F^{(1)})\frac{n\tau_c}{2}\right\} \\ &\times \exp\left\{-i(\tilde{\mathcal{H}}_F^{(0)} + \tilde{\mathcal{H}}_F^{(1)})\frac{n\tau_c}{2}\right\},\end{aligned} \tag{25}$$

where the fact that $\tilde{\mathcal{H}}^{(1)}$ change the sign when the r.f. phase is inverted was used. Additionally, as the pulse sequence was designed to fulfil the condition $\tilde{\mathcal{H}}_B^{(0)} = -\tilde{\mathcal{H}}_F^{(0)}$, we can write

$$\begin{aligned}\mathcal{U}(2n\tau_c) = &\exp\left\{-i(-\tilde{\mathcal{H}}_F^{(0)} - \tilde{\mathcal{H}}_B^{(1)})\frac{n\tau_c}{2}\right\} \\ &\times \exp\left\{-i(-\tilde{\mathcal{H}}_F^{(0)} + \tilde{\mathcal{H}}_B^{(1)})\frac{n\tau_c}{2}\right\} \\ &\times \exp\left\{-i(\tilde{\mathcal{H}}_F^{(0)} - \tilde{\mathcal{H}}_F^{(1)})\frac{n\tau_c}{2}\right\} \\ &\times \exp\left\{-i(\tilde{\mathcal{H}}_F^{(0)} + \tilde{\mathcal{H}}_F^{(1)})\frac{n\tau_c}{2}\right\}.\end{aligned} \tag{26}$$

It is straightforward to see from Eq. (26) that if $\tilde{\mathcal{H}}_B^{(1)} = \tilde{\mathcal{H}}_F^{(1)}$, the following equalities hold:

$$\mathcal{U}_B^{(+)} = \left(\mathcal{U}_F^{(-)}\right)^{-1}, \quad \mathcal{U}_B^{(-)} = \left(\mathcal{U}_F^{(+)}\right)^{-1}, \tag{27}$$

resulting in the absence of evolution ($\mathcal{U}(2n\tau_c) = \mathcal{I}$). Therefore, the evolution during the pulse sequence is directly related with the fact that the *first order average Hamiltonians* are unequal during the forward and backward evolutions. In Fig. 7, the factors h_j multiplying the commutators in Eq. (22) are plotted against the scaling factor k. The data points were calculated with values of $k = 0, \pm 1/n$ for $n = 2$–8 and the effective frequency used in the experiments. From the curves, it is evident that $\tilde{\mathcal{H}}_B^{(1)} \neq \tilde{\mathcal{H}}_F^{(1)}$.

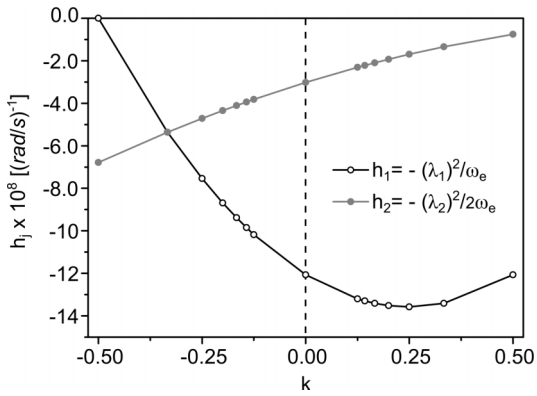

FIG. 7. Pre-factors of the commutators in Eq. (22), h_1, h_2 vs. k. The asymmetry of the curves with respect to $k = 0$ results in the difference between forward and backward evolutions during PRL echo.

4. Numerical simulations

In this part, we present numerical simulations in order to investigate the effects of the first order average Hamiltonian in the PRL echo pulse sequence. The calculations were performed in a system consisting in 8 spins-1/2, each occupying a vertex on a cube of side $a = 0.35$ nm with. The resulting distribution of dipolar coupling strengths is such that max $|d_{ij}| = 2.78$ kHz. Figures 8(a)–8(c) display Loschmidt echoes with different k and effective field intensities (or equivalently ω_e). The curves were calculated by means of the propagators of Eq. (26), where the first order Hamiltonian norm (i.e., h_j's) corresponds to the values shown in Fig. 7. For all effective frequencies, the overall behaviour observed in the experiments are reproduced (see Fig. 5), despite the time scale, due to the reduced size of the system used in the simulations. It is worthy to remark that the echo decay is more pronounced as ω_e decreases, because the values $\| \tilde{\mathcal{H}}^{(1)} \| \propto 1/\omega_e$ become larger.

5. The limiting case k = 0

The curves corresponding to $k = 0$, i.e., the Lee-Goldburg condition, show no evolution independently of the effective field (see Figs. 8(a)–8(c)). This is consistent with the fact that $\tilde{\mathcal{H}}_B^{(1)} = \tilde{\mathcal{H}}_F^{(1)}$ in this case. However, the experimental results have shown that the $k = 0$ case presents a decay rate with a time-scale comparable to the $k \neq 0$ curves, as seen in Fig. 5(a). To find out the origin of this decay, it is useful to compare the exact dynamics with its first order average Hamiltonian.

The propagator of the forward block in terms of the average Hamiltonian expansion in the tilted frame (i.e., neglecting β pulses) results in the Identity operator,

$$\mathcal{U}(n\tau_c) = \exp\left\{i\,\overline{\mathcal{H}}_F^{(1)}\frac{n\tau_c}{2}\right\} \times \exp\left\{-i\,\overline{\mathcal{H}}_F^{(1)}\frac{n\tau_c}{2}\right\} = \mathcal{I}, \tag{28}$$

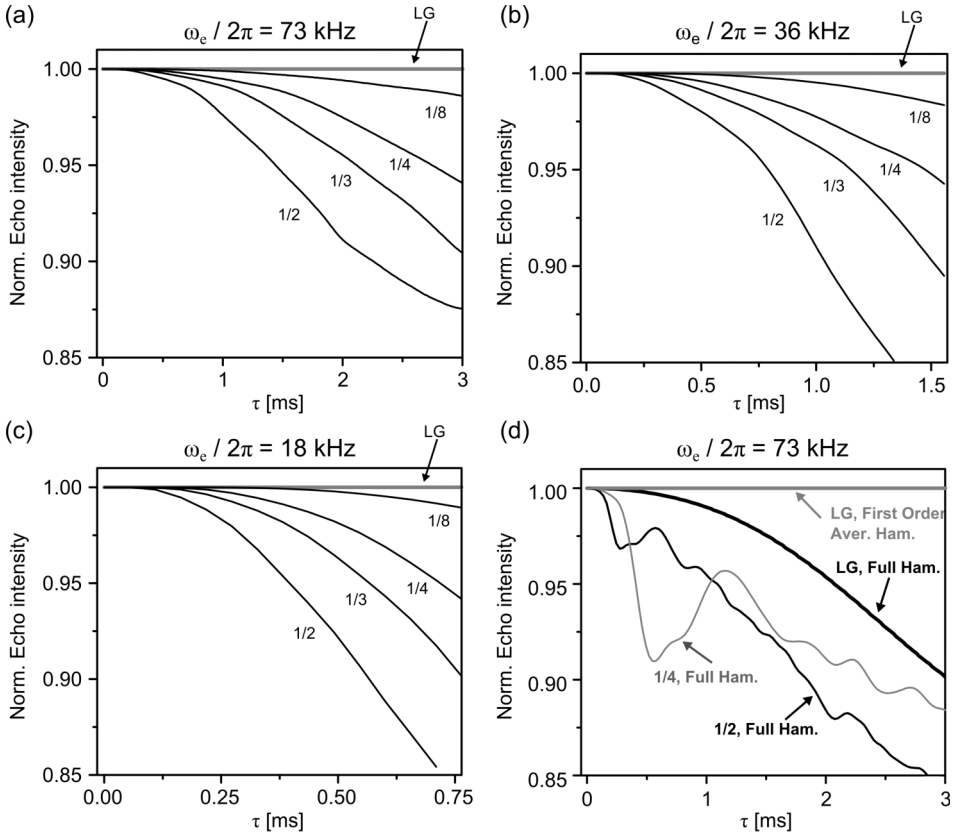

FIG. 8. Numerical simulations for a system of eight spins. Normalized echo intensities are plotted against τ for different scaling dipolar factors. From (a)-(c), the system evolves according to Eq. (26) for different values of the effective field strength. (d) Two curves with $k = 0$ calculated either with the first order Average Hamiltonian or with the full Hamiltonian in the toggling frame. Curves calculated with the full Hamiltonian for two representative values of k are included to show that the echo in the LG condition decays in the same time scale.

since, as above mentioned, the first order changes its sign when the r.f. changes the phase. On the other hand, the propagator in terms of the full Hamiltonian of Eq. (3) and Table I is

$$\mathcal{U}(n\tau_c) = \exp\left\{-i\left(-\mathcal{H}_e + \sum_{j\neq 0}\lambda_j\mathcal{H}_j\right)\frac{n\tau_c}{2}\right\} \times \exp\left\{-i\left(\mathcal{H}_e + \sum_{j\neq 0}\lambda_j\mathcal{H}_j\right)\frac{n\tau_c}{2}\right\}. \quad (29)$$

Notice that the factors λ_j are non-zero when $k = 0$ (see Fig. 1(b)), and are independent of the r.f. phase. Thus, both non-commuting arguments in the exponentials of Eq. (29) produce a global evolution which is independent of the phase change of the effective field, being responsible for the LE decay. Therefore, while Eq. (29) describes an overall decay, Eq. (28) yields a fake identity. This is emphasized in Fig. 8(d), where calculations with Eqs. (28) and (29) are presented together for the maximum effective field intensity used in the simulations. In contrast, when $|k| \neq 0$, the presence of the dominant secular term, $\lambda_0\mathcal{H}_0 = \overline{\mathcal{H}}^{(0)}$, makes the differences between Eqs. (28) and (29) irrelevant. This is observed in both curves corresponding to $|k| = 1/2, 1/4$ calculated with the full Hamiltonian in the same figure. In our small spin system, there are oscillations associated with $\mathcal{H}_e$ and the secular part of the dipolar Hamiltonian that makes the quantification of the decays less clear. These unavoidable finite size effects should smear out if one could solve much bigger systems.[6,47] In any case, the ordering of the decays obtained with the first order average Hamiltonian confirm the effectiveness of the scaling in the dynamics.

IV. CONCLUSIONS

In this work, we have performed Loschmidt echo experiments to study decoherence in a many-spin system under a scaled dipolar Hamiltonian. With this purpose, a symmetrical time-reversal pulse sequence denominated PRL echo has been introduced. The time reversion was obtained through two steps of evolution characterized by the secular part of the dipolar Hamiltonian, scaled down with a factor $|k|$ and opposite signs. The variable $|k|$ can be varied at the discretion of the experimenter, in the range $0 \leq |k| \leq 1/2$.

The experimental results for the LE's showed a spreading of the decay rates that correlates directly to the scaling factors $|k|$. In other words, the decoherence is partially governed by the scaling factors of the coherent dynamics. Several tests on the pulse sequence performance were used to demonstrate that, in the range of our experimental values, the r.f. inhomogeneities can be safely disregarded and therefore the behaviour observed reflects the quantum dynamical complexity of the spin-system. Notice that this set of experiments were done varying the rf power in order to maintain fixed the effective field that determines the relative importance of the truncated terms. This is particularly relevant when considering the small $|k|$ values. The results were complemented with a series of tests using the magic echo pulse sequence (data not shown). Although the r.f. field strength modifies the truncation errors during the reversed dynamics, the observed decays did not

show a marked dependence on this parameter. A full comparison of the performance of both pulse sequences is out of the scope of this article and will be presented in a future publication.

The Average Hamiltonian Theory was applied to provide an insight into the spin dynamics during the pulse sequence. The calculations were performed for every single r.f. block, in contrast to the most widely used form. The first order of the average Hamiltonian numerically computed for a 8-spin system showed decay rates that progressively decrease as the secular Hamiltonian (see Eq. (3)) becomes weaker. The simulated echoes, however, do not decay when $k = 0$. This marks a deep contrast with the experiments where strong overall decoherence rate is observed for the whole range of k values. Thus, we proceed to include reasonable errors in the pulse sequence to analyse their importance in the overall echoes decay. Their influence is present but in no way could account for the experimental observations. Notably, this term $\tilde{\mathcal{H}}^{(1)}$, neglected by conventional calculations, yielded an explanation for the ordering of the experimental decoherence rates. While we were expecting that the effective Hamiltonian that provides many spin complexity would also be controlling decoherence, the experiments only partially follows this trend. Thus, the mechanism responsible for the dominant decay, which is independent of the rf strength or the scaling factor of the zeroth order average Hamiltonian, remains unknown. At this point, the only term that has not been analysed in detail so far is the original non-secular terms in Eq. (1), and this opens an avenue for theoretical analysis.

Among the list of experiments that could help understanding the influence of the complete Hamiltonian in this dominant decoherence are time reversal experiments in single crystals at different orientations, the study of the developing of multiple quantum coherences during the dynamics, and the scaling of the dipolar dynamics through the reduced evolution of the polarization echo procedure.[21] All these proposals can be directly combined with the PRL echo sequence both for initial magnetization parallel or perpendicular to the effective field to shed further light on dynamical instability and the origin of decoherence in many-body quantum systems.

ACKNOWLEDGMENTS

This work was conducted with partial support of ANPCyT, CONICET, MiNCyT-Cor, and SeCyT-UNC. The authors would like to thank P. R. Zangara for the fruitful discussions during the preparation of this manuscript.

APPENDIX: FIRST ORDER AVERAGE HAMILTONIAN TERMS

In this appendix, we present the full description of the first order average Hamiltonian in terms of the product operators. Equations (20) and (21) show the relationship between the first order and the secular and non-secular Hamiltonians, in the tilted frame defined by the radiofrequency. The expression of Eq. (20) can be recast as

TABLE III. Functional form of $\mathcal{A}$'s and $\mathcal{B}$'s.

Term	Structure
$\mathcal{A}_1$	$\delta_{il}(2I_k^Z I_i^+ I_j^Z + 2I_k^Z I_i^- I_j^Z + \frac{1}{2} I_k^+ I_i^+ I_j^- - \frac{1}{2} I_k^- I_i^+ I_j^- + I_k^Z I_i^Z I_j^- - \frac{1}{2} I_k^+ I_i^- I_j^+ + \frac{1}{2} I_k^- I_i^- I_j^+ + I_k^Z I_i^Z I_j^+)$
$\mathcal{A}_2$	$\delta_{jl}(2I_i^Z I_k^Z I_j^+ + 2I_i^Z I_k^Z I_j^- - \frac{1}{2} I_i^+ I_k^+ I_j^- + \frac{1}{2} I_i^+ I_k^- I_j^- + \frac{1}{2} I_i^- I_k^+ I_j^+ - \frac{1}{2} I_i^- I_k^- I_j^+ + I_i^+ I_k^Z I_j^Z + I_i^- I_k^Z I_j^Z)$
$\mathcal{A}_3$	$\delta_{ik}(2I_i^+ I_l^Z I_j^Z + 2I_i^- I_l^Z I_j^Z + I_i^Z I_l^Z I_j^- + \frac{1}{2} I_i^+ I_l^+ I_j^- - \frac{1}{2} I_i^+ I_l^- I_j^- + I_i^Z I_l^Z I_j^- + \frac{1}{2} I_i^+ I_l^- I_j^+ + \frac{1}{2} I_i^- I_l^- I_j^+)$
$\mathcal{A}_4$	$\delta_{jk}(2I_i^Z I_k^+ I_l^Z + 2I_i^Z I_k^- I_l^Z + I_i^+ I_k^Z I_l^Z - \frac{1}{2} I_i^+ I_k^- I_l^+ + \frac{1}{2} I_i^+ I_k^- I_l^- + I_i^- I_k^Z I_l^Z + \frac{1}{2} I_i^- I_k^+ I_l^+ - \frac{1}{2} I_i^- I_k^+ I_l^-)$
$\mathcal{B}_1$	$\delta_{il}\left\{2I_k^+ I_i^+ I_j^Z + 2I_k^- I_i^- I_j^Z + I_k^- I_i^Z I_j^- + I_k^+ I_i^Z I_j^+\right\}$
$\mathcal{B}_2$	$\delta_{jl}\left\{2I_i^Z I_k^+ I_j^+ + 2I_i^Z I_k^- I_j^- + I_i^+ I_k^+ I_j^Z + I_i^- I_k^- I_j^Z\right\}$
$\mathcal{B}_3$	$\delta_{ik}\left\{2I_i^+ I_l^+ I_j^Z + 2I_i^- I_l^- I_j^Z + I_i^Z I_l^+ I_j^+ + I_i^Z I_l^- I_j^-\right\}$
$\mathcal{B}_4$	$\delta_{jk}\left\{2I_i^Z I_j^+ I_l^+ + 2I_i^Z I_j^- I_l^- + I_i^+ I_j^Z I_l^+ + I_i^- I_j^Z I_l^-\right\}$
C_1	$\delta_{il}\left\{2I_k^Z I_i^Z I_j^Z - I_k^- I_i^+ I_j^Z - I_k^Z I_i^- I_j^+\right\}$
C_2	$\delta_{jl}\left\{2I_i^Z I_k^Z I_j^Z - I_i^+ I_k^Z I_j^- - I_i^Z I_k^- I_j^+\right\}$
C_3	$\delta_{ik}\left\{2I_i^Z I_l^Z I_j^Z - I_i^+ I_l^- I_j^Z - I_i^- I_l^Z I_j^+\right\}$
C_4	$\delta_{jk}\left\{2I_i^Z I_j^Z I_l^Z - I_i^+ I_j^- I_l^Z - I_i^Z I_j^+ I_l^-\right\}$
$\mathcal{D}_1$	$\delta_{il}\, 2I_k^- I_i^Z I_j^+$
$\mathcal{D}_2$	$\delta_{jl}\, 2I_i^+ I_k^- I_j^Z$
$\mathcal{D}_3$	$\delta_{ik}\, 2I_i^Z I_l^- I_j^+$
$\mathcal{D}_4$	$\delta_{jk}\, 2I_i^+ I_j^Z I_l^-$

$$\overline{\mathcal{H}}^{(1)}_{0,M} = -\frac{3\lambda_0\lambda_1}{\omega_e} \sum_{i<j;k<l} d_{ij}d_{kl}\,(\mathcal{A}_1 + \mathcal{A}_2 + \mathcal{A}_3 + \mathcal{A}_4) - \frac{3\lambda_0\lambda_2}{2\,\omega_e} \sum_{i<j;k<l} d_{ij}d_{kl}\,(\mathcal{B}_1 + \mathcal{B}_2 + \mathcal{B}_3 + \mathcal{B}_4)\,. \quad \text{(A1)}$$

On the other hand, Eq. (21) can be rearranged as

$$\overline{\mathcal{H}}^{(1)}_{M^2} = -\frac{9(\lambda_1)^2}{\omega_e} \sum_{i<j;k<l} d_{ij}d_{kl}\,(C_1 + C_2 + C_3 + C_4) - \frac{9(\lambda_2)^2}{2\,\omega_e} \sum_{i<j;k<l} d_{ij}d_{kl}\,(\mathcal{D}_1 + \mathcal{D}_2 + \mathcal{D}_3 + \mathcal{D}_4)\,. \quad \text{(A2)}$$

The terms $\mathcal{A} - \mathcal{D}$ are summarized in Table III.

[1]J. L. Lebowitz, Phys. Today **46**(9), 32 (1993).
[2]W. H. Zurek, Rev. Mod. Phys. **75**, 715 (2003).
[3]R. M. Serra and I. S. Oliveira, Philos. Trans. R. Soc., A **370**, 4615 (2012).
[4]H. M. Pastawski, P. R. Levstein, and G. Usaj, Phys. Rev. Lett. **75**, 4310 (1995).
[5]H. M. Pastawski, G. Usaj, and P. R. Levstein, Chem. Phys. Lett. **261**, 329 (1996).
[6]W. H. Zurek, F. Cucchietti, and J. Paz, Acta Phys. Pol., B **38**, 1685 (2007).
[7]G. A. Álvarez, E. P. Danieli, P. R. Levstein, and H. M. Pastawski, Phys. Rev. A **82**, 012310 (2010).
[8]G. Roumpos, C. Master, and Y. Yamamoto, Phys. Rev. B **75** (2007).
[9]H.-B. Liu, J.-H. An, C. Chen, Q.-J. Tong, H.-G. Luo, and C. H. Oh, Phys. Rev. A **87**, 052139 (2013).
[10]A. Fedorov and L. Fedichkin, J. Phys.: Condens. Matter **18**, 3217 (2006).
[11]C. A. Ryan, J. Emerson, D. Poulin, C. Negrevergne, and R. Laflamme, Phys. Rev. Lett. **95**, 250502 (2005).
[12]P. C. Maurer, G. Kucsko, C. Latta, L. Jiang, N. Y. Yao, S. D. Bennett, F. Pastawski, D. Hunger, N. Chisholm, M. Markham, D. J. Twitchen, J. I. Cirac, and M. D. Lukin, Science **336**, 1283 (2012).
[13]E. L. Hahn, Phys. Rev. **80**, 580 (1950).
[14]W. K. Rhim, A. Pines, and J. S. Waugh, Phys. Rev. Lett. **25**, 218 (1970).
[15]H. Cho, T. Ladd, J. Baugh, D. Cory, and C. Ramanathan, Phys. Rev. B **72**, 054427 (2005).

[16]G. Boutis, P. Cappellaro, H. Cho, C. Ramanathan, and D. Cory, J. Magn. Res. **161**, 132 (2003).
[17]S. W. Morgan, V. Oganesyan, and G. S. Boutis, Phys. Rev. B **86**, 214410 (2012).
[18]S. Zhang, B. H. Meier, and R. R. Ernst, Phys. Rev. Lett. **69**, 2149 (1992).
[19]P. R. Levstein, G. Usaj, and H. M. Pastawski, J. Chem. Phys. **108**, 2718 (1998).
[20]P. R. Levstein, A. K. Chattah, H. M. Pastawski, J. Raya, and J. Hirschinger, J. Chem. Phys. **121**, 7313 (2004).
[21]G. Usaj, H. M. Pastawski, and P. R. Levstein, Mol. Phys. **95**, 1229 (1998).
[22]E. Rufeil-Fiori and H. Pastawski, Chem. Phys. Lett. **420**, 35 (2006).
[23]H. Pastawski, P. Levstein, G. Usaj, J. Raya, and J. Hirschinger, Physica A **283**, 166 (2000).
[24]C. M. Sánchez, P. Levstein, R. Acosta, and A. Chattah, Phys. Rev. A **80**, 012328 (2009).
[25]C. E. González, H. H. Segnorile, and R. C. Zamar, Phys. Rev. E **83**, 011705 (2011).
[26]R. Jalabert and H. Pastawski, Phys. Rev. Lett. **86**, 2490 (2001).
[27]F. M. Cucchietti, D. A. R. Dalvit, J. P. Paz, and W. H. Zurek, Phys. Rev. Lett. **91**, 210403 (2003).
[28]A. Goussev, R. Jalabert, H. M. Pastawski, and D. Wisniacki, Scholarpedia **7**, 11687 (2012).
[29]P. R. Zangara, A. D. Dente, P. R. Levstein, and H. M. Pastawski, Phys. Rev. A **86**, 012322 (2012).
[30]S. A. Moiseev, Phys. Rev. A **88**, 012304 (2013).
[31]P. R. Zangara, A. D. Dente, A. Iucci, P. R. Levstein, and H. M. Pastawski, Phys. Rev. B **88**, 195106 (2013).
[32]G. A. Álvarez and D. Suter, Phys. Rev. A **84**, 012320 (2011).
[33]G. A. Álvarez, D. Suter, and R. Kaiser, Science **349**, 846 (2015).
[34]J. Baum and A. Pines, J. Am. Chem. Soc. **108**, 7447 (1986).
[35]C. A. Michal and R. Tycko, J. Chem. Phys. **114**, 409 (2001).
[36]C. Ramanathan, H. Cho, P. Cappellaro, G. Boutis, and D. Cory, Chem. Phys. Lett. **369**, 311 (2003).
[37]C. Ramanathan, P. Cappellaro, L. Viola, and D. G. Cory, New J. Phys. **13**, 103015 (2011).
[38]H. Krojanski and D. Suter, Phys. Rev. Lett. **93**, 090501 (2004).
[39]C. M. Sánchez, H. M. Pastawski, and P. R. Levstein, Physica B **398**, 472 (2007).
[40]C. M. Sánchez, R. H. Acosta, P. R. Levstein, H. M. Pastawski, and A. K. Chattah, Phys. Rev. A **90**, 042122 (2014).
[41]E. Rufeil-Fiori, C. M. Sánchez, F. Oliva, H. M. Pastawski, and P. R. Levstein, Phys. Rev. A **79**, 032324 (2009).
[42]P. R. Levstein, G. Usaj, H. M. Pastawski, J. Raya, and J. Hirschinger, J. Chem. Phys. **115**, 6285 (2000).
[43]A. K. Chattah and P. R. Levstein, J. Chem. Phys. **124**, 124513 (2006).
[44]C. P. Slichter, *Principles of Magnetic Resonance* (Springer-Verlag, Berlin, New York, 1990).
[45]W.-K. Rhim, A. Pines, and J. S. Waugh, Phys. Rev. B **3**, 684 (1971).
[46]A. Pines and J. S. Waugh, J. Magn. Reson. (1969) **8**, 354 (1972).
[47]P. R. Zangara, D. Bendersky, and H. M. Pastawski, Phys. Rev. A **91**, 042112 (2015).
[48]J. Baum, M. Munowitz, A. N. Garroway, and A. Pines, J. Chem. Phys. **83**, 2015 (1985).
[49]I. Schnell and H. W. Spiess, J. Magn. Reson. **151**, 153 (2001).
[50]G. A. Álvarez, R. Kaiser, and D. Suter, Ann. Phys. **525**, 833 (2013).
[51]A. Bielecki, A. Kolbert, and M. Levitt, Chem. Phys. Lett. **155**, 341 (1989).
[52]R. R. Ernst, G. Bodenhausen, and A. Wokaun, *Principles of Nuclear Magnetic Resonance in One and Two Dimensions* (Clarendon Press, Oxford University Press, Oxford, New York, 1987).
[53]U. Haeberlen and J. S. Waugh, Phys. Rev. **175**, 453 (1968).